Chemical Physics 446 (2015) 7–12

Contents lists available at ScienceDirect

Chemical Physics

journal homepage: www.elsevier.com/locate/chemphys

Shear banding in simulated telechelic polymers

Joris Billen, Mark Wilson, Arlette R.C. Baljon *

Department of Physics, San Diego State University, San Diego, CA 92128, USA

ARTICLE INFO

Article history:
Received 30 June 2014
In final form 2 November 2014
Available online 8 November 2014

Keywords:
Molecular dynamics
Polymers
Self-assembly

ABSTRACT

The response of simulated telechelic polymers to shear is investigated. End groups of short polymeric chains form temporary junctions that are continuously broken and formed over time. As in experiments, two shear bands coexist for some shear rates. This allows us to study the microscopic differences between these shear bands. We find that the lifetime of a junction is lower in the high shear rate band. In addition, the average aggregate size is lower in this band since more dangling chains exist. Microstructural differences between the sheared and unsheared system are reported as well. Some of the chains, that bridge between two aggregates before shear is applied, form loops that connect with both ends to the same aggregate instead. In addition and more importantly, an increase of chains connecting the same two aggregates is observed. Such restructuring lowers the network connectivity and hence the stress needed to shear the system.

1. Introduction

Shear banding is a common phenomenon in many complex systems. When these systems are sheared at a rate that is higher than the inverse relaxation time, homogeneous flow becomes unstable. As a consequence two bands with different shear rates form. Although this effect has been observed in a wide variety of systems, such as emulsions, dispersions, granular materials, and foams, it has been most extensively studied experimentally in wormlike micelles [1–9]. A theoretical explanation for shear banding lies in the behavior of the underlying constitutive curve, relating shear stress σ to the shear rate $\dot{\gamma}$ [4,8,10]. In homogeneous flow, there is a range of shear rates for which the curve decreases, indicating a mechanical instability. Hence, it is predicted that the flow splits in two bands and the stress plateaus. This theory also predicts the width of the bands; the so-called lever rule states that the location of the interface between both bands changes gradually with the applied shear rate, while the local shear rates in both bands are constant. The interface is located such that

$$\dot{\gamma} = \alpha_1 \dot{\gamma}_1 + \alpha_2 \dot{\gamma}_2 \tag{1}$$

where α_1 and α_2 are the relative widths of the shear bands. Although some experiments confirm the lever rule [3,6], others indicate that the picture of two smooth bands separated by a stable interface is insufficient to explain the complex behavior at the interface [1,7,9,11]. The position of the interface seems to fluctuate and drift, long after the initial start of the shear.

Shear banding in associating telechelic polymers has been studied more recently [12–14]. From these studies, it is clear that shear banding is a complex problem that is still poorly understood. The behavior depends strongly on many parameters such as temperature, concentration, chemical structure, along with the details on how the flow curve was obtained [9,12]. Sometimes three bands are observed.

Simulations can help in shedding new light on some aspects of the problem. They allow us to study the structural properties at the microscopic scale in each shear band. We have employed a toy model of associating polymers. It consists of short polymer chains, whose end groups can aggregate together. Extensive studies of the equilibrium phase behavior of this model have been published [15,16]. Within the following, we will report on the topological changes of a polymer network, observed in a sheared system. If both end groups of the chain are part of the same aggregate, a loop is formed. If both end groups are part of different aggregates, the polymer chain forms a bridge. There are reports that the number of loops increases when shear is applied. The number of elastic active bridges decreases and as a result the stress decreases [3,15,17,18]. We investigate other topological differences as well. For example, aggregates could be linked by more than one chain. Such subtle structural features are hard to observe experimentally. Hence, we believe that our results provide new insight.

2. Simulation methods

The model used for simulating telechelic polymers is a hybrid model consisting of a molecular dynamics simulation (MDS) with

* Corresponding author.

http://dx.doi.org/10.1016/j.chemphys.2014.11.001
0301-0104/

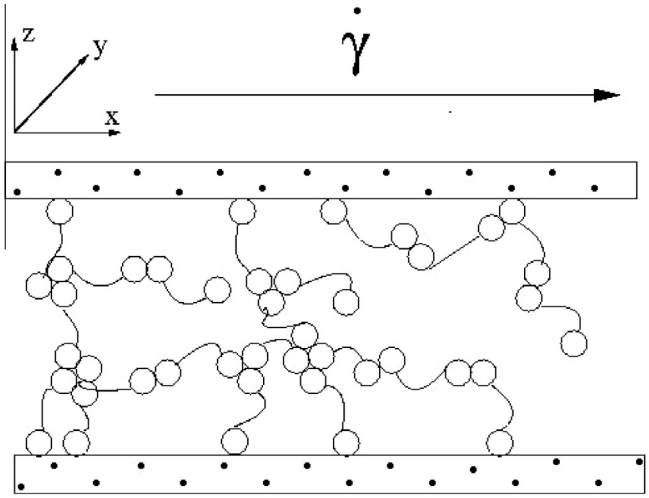

Fig. 1. Schematic of the simulation cell. The top wall is moved to the right at a constant rate. Stress is calculated from the interactions between the polymers and top wall. The junctions between the spheres can break and reform. The simulation is performed in 3 dimensions.

a Monte Carlo (MC) step and has been described in earlier work [15,16]. To model polymer chains, a standard bead-spring model [19] is used. Any two beads in the system experience a Lennard–Jones potential

$$U_{ij}^{LJ} = 4\varepsilon\left[\left(\frac{\sigma}{r_{ij}}\right)^{12} - \left(\frac{\sigma}{r_{ij}}\right)^{6} - \left(\frac{\sigma}{r_c}\right)^{12} + \left(\frac{\sigma}{r_c}\right)^{6}\right] \quad \text{for } r_{ij} < r_c \tag{2}$$

that has been shifted and is purely repulsive ($r_c = 2^{1/6}$). All units in this paper are expressed in terms of the Lennard–Jones units: length (σ), energy (ε), and time $\tau = \sigma(\frac{m}{\varepsilon})^{1/2}$. Neighboring beads within the polymer chain experience a strong anharmonic FENE spring potential

$$U_{ij}^{\text{FENE}} = -\frac{1}{2}kR_0^2 \ln\left[1 - \left(\frac{r_{ij}}{R_0}\right)^2\right] \quad \text{for } r_{ij} < \mathrm{R}_0 \tag{3}$$

with $k = 30$ and $R_0 = 1.5$. This standard bead-spring model has been extended to include a MC step which models the associative properties of the polymer chains [15,20]. During a MC step, junctions between end groups of chains can either be formed or broken. A junction between end groups is modeled as the FENE potential from Eq. (3) and a negative association energy equal to −22. Each attempt to break and form junctions is accepted or rejected based on the energy difference between the old and new configuration. Note that if the FENE bonds are stretched, they are more likely to break in an MC attempt.

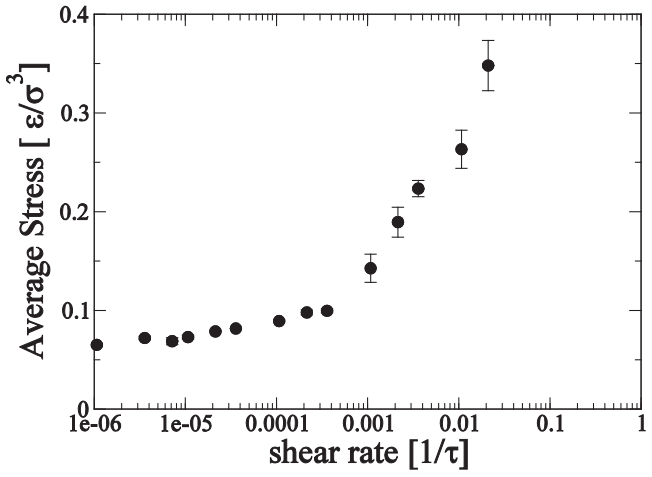

Fig. 2. Average stress in the steady state as a function of shear rate. Error bars are obtained from the standard deviation of different runs, independently cooled from $T = 1.5$.

The equations of motions are integrated using a fifth-order Gear predictor–corrector algorithm with $\delta t = 0.005\ \tau$. The temperature is controlled by coupling the system to a heat bath. All results shown in this work are at a temperature $T = 0.35$ in the gel state [15]. The system is initially cooled at a rate of 2500 τ per $\Delta T = 0.1$ from a high sol state at $T = 1.5$. The system is always equilibrated for 5000 τ at $T = 0.35$ before shear is applied. Results are averaged over several shear runs, obtained using initial states that resulted from cooling different high temperature states. The simulation cell has dimensions $23.69 \times 20.54 \times 27.84$ and contains 1000 chains. Each chain is 8 beads long. Hence, the volume fraction of the simulation cell that is occupied equals 0.31. A schematic of the system is shown in Fig. 1. It is confined by two solid walls in the z-direction and has periodic boundary conditions in the other two directions. 5% of the end groups are permanently grafted to the walls. This allows us to perform shear experiments in which the top wall is

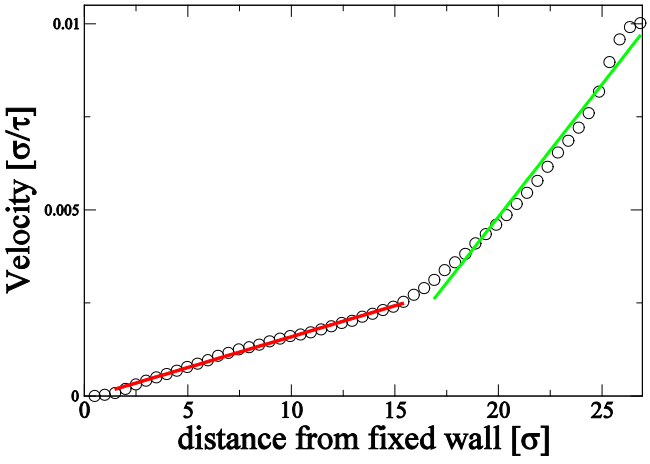

Fig. 3. Velocity profile for an applied shear rate of $\dot{\gamma} = 3.59 \times 10^{-4}\tau^{-1}$. The slopes for both shear rate bands are shown as bold lines and indicate shear rates of $1.6 \times 10^{-4}\,\tau^{-1}$ and $7.11 \times 10^{-4}\,\tau^{-1}$.

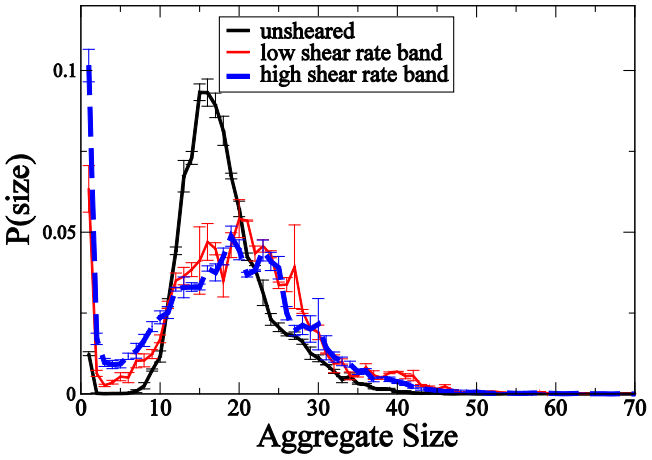

Fig. 4. Aggregate size distribution for the unsheared system (dotted), the high shear rate band (solid), and the low shear-rate band (dashed).

Table 1
Comparison of quantities in the unsheared and sheared system. For the sheared system measurements were made in slabs 4 σ thick located 1.8 σ from the walls.

	Unsheared	Low shear rate band	High shear rate band
End-to-end distance [σ]	3.9 ± 0.2	4.81 ± 0.09	4.75 ± 0.06
Bead concentration [beads/σ^3]	0.62 ± 0.01	0.62 ± 0.01	0.61 ± 0.01
Average aggregate size	17.9 ± 0.2	19.6 ± 0.2	17.8 ± 0.6
Aggregate density [aggregates/σ^3]	0.0086 ± 0.0004	0.0079 ± 0.0004	0.0089 ± 0.0002
Lifetime of junctions [τ]	(1895 ± 153) 10^3	(11.220 ± 3.145) 10^3	(3.645 ± 0.625) 10^3

moved with a constant velocity. The shear rate then equals the velocity divided by the distance between the walls.

3. Results and discussion

The shear rate is varied between 1.79×10^{-6} τ^{-1} and 3.58×10^{-2} τ^{-1}. Note that the inverse relaxation time of the system, obtained from diffusion data in earlier work [15] equals 9.455×10^{-8} τ^{-1}. Hence, all shear rates under consideration are larger than the inverse relaxation time. The force required to move the upper wall is obtained from the interactions between the wall and polymer beads. The stress, measured as force per unit wall area, initially increases and reaches a maximum when the strain is approximately 1.5, more or less independent of the shear rate. At that point the system yields and subsequently the stress starts to fluctuate around a lower average stress value. Fig. 2 shows this average value as a function of shear rate. Note that at low shear rates the stress is only slightly increasing, while a strong increase is observed for the higher rates. Even though a perfect plateau in the stress is not observed, we have investigated the data further and indeed find shear banding. A slight slope in the stress, in the shear banding regime, has also been observed in experiments on wormlike micelles [3,7]. We found that shear bands were most clearly visible at a shear rate of 3.6×10^{-4} τ^{-1}. Since the goal of this work is to study the microscopic structural features of a shear banding system, we concentrate on this shear rate. Fig. 3 shows the flow profile in the system. A high shear rate band near the moving wall and low shear rate band near the steady wall can be observed. Data are averaged over 7 different runs, each of which is obtained by cooling a different high temperature configuration to the gel state at $T = 0.35$ and subsequently applying shear. Note that the shear rates of the bands are approximately a factor of 4.3 different (1.6×10^{-4} τ^{-1} and 7.11×10^{-4} τ^{-1} respectively). In micellar systems the difference tends to be much higher. However, the factor 4.3 is in reasonable agreement with the experiments by Sprakel et al. on telechelic polymers [13].

Table 1 compares several microscopic properties in the unsheared system, high shear rate band, and low shear rate band. The average position of the interface between the bands as shown in Fig. 3 is at 17.1 ± 1.0. However, the actual position fluctuates over time. Therefore, data in the high and low shear rate bands are obtained from averages over two slabs, located between 1.8 σ and 5.8 σ from each wall. The dimensions and locations of these slabs were chosen so that they are always located in the appropriate shear band. As expected, the end-to-end distance of the polymer chains increases under shear. The stretch is identical in both bands, though. The concentration of the beads is not affected by the shear. However, the high shear rate band contains more aggregates, which are on average smaller in size. A more detailed comparison of the aggregate sizes in the unsheared system and the bands of high and low shear rate is given in Fig. 4, which shows the aggregate size distribution. As expected in the unsheared gel state. The distribution peaks around a preferred value of approximately 16 chain end groups. After the application of shear, this value increases to approximately 22. Such shear-induced aggregation in associating polymers has been reported previously in experiments and in simulations [17,21]. Most noticeable is the fact that the number of very large aggregates (size 25 and up) is strongly increased in the sheared system. Visualization of the largest aggregates shows an elongated structure. The difference between the high shear rate and low shear rate bands is the number of small aggregates and single end groups. These are more frequent in the high shear rate band. This causes the average aggregate size to be lower.

In order to investigate the origin of the difference in the aggregate size distribution of the sheared system, we study the rates at which aggregates form and break. A detailed study of these rates for the unsheared system has been published recently [22]. In Fig. 5 q_f equals the number of times that an aggregate of size k

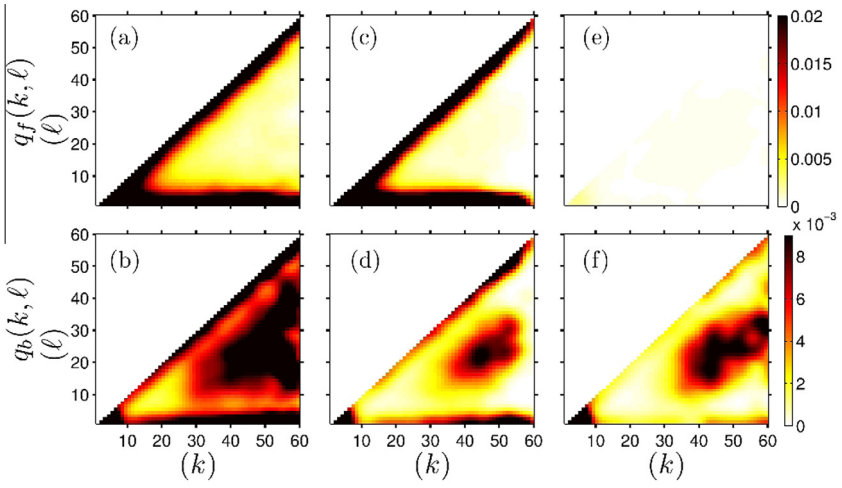

Fig. 5. Aggregate association (q_f) and dissociation (q_b) rates in the high shear rate band (a, b) and low shear rate band (c, d) when $\dot{\gamma} = 3.59 \times 10^{-4}\tau^{-1}$. Rates are compared to those in the unsheared system (e, f).

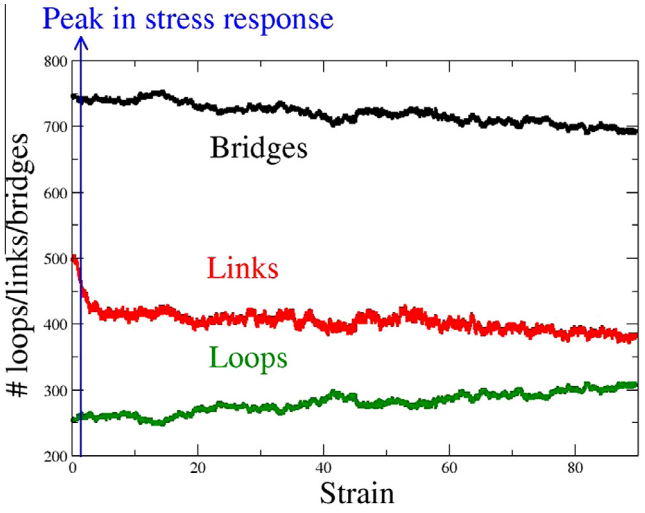

Fig. 6. Change in the number of loops, bridging chains (bridges), and links after applying a shear at $\dot{\gamma} = 3.59 \times 10^{-4}\tau^{-1}$. The links can contain one or more bridging chains.

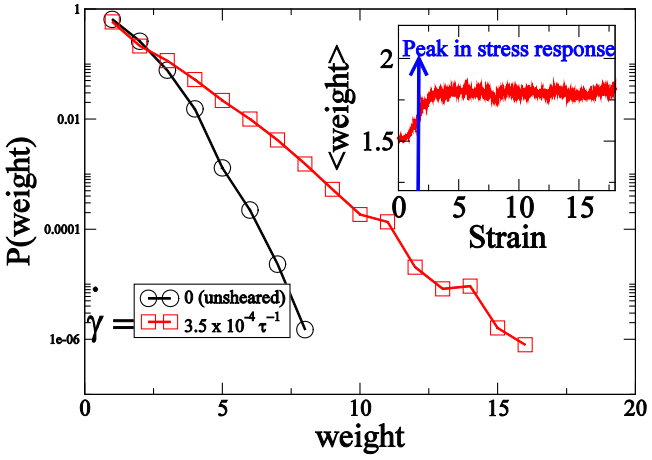

Fig. 7. Probability of having a link consisting of a certain weight versus weight for unsheared system (circles), and sheared system at $\dot{\gamma} = 3.59 \times 10^{-4}\tau^{-1}$ (squares). The inset shows the average weight as function of applied strain. The arrow indicates the peak in the stress overshoot.

forms by combining one of size ℓ and size $k-\ell$ in a time period τ. This number is normalized by the number of aggregates of size ℓ and $k-\ell$. Also shown is the probability that an aggregate of size k breaks into smaller ones with sizes ℓ and $k-\ell$ (q_b). As can be seen, the chance of formation is strongly increased under shear. In particular aggregates grow by adding single end groups or very small aggregates (less than size 5). Those small aggregates are also much more likely to break off under shear. However, break rates are also very high for aggregate sizes around 40 or 50. These tend to break into two nearly equal sized aggregates, close to the preferential size of the aggregate distribution. This effect is stronger in the high shear rate band. However, due to the relative low number of such large aggregates, the main difference between the shear bands is the higher likelihood that small aggregates break away in the high shear rate band. This process of removing a single end group or small aggregate and combining it with the same or another aggregate facilitates the shear. Another way to look at the dynamics of the system is through the lifetime of the FENE junctions between the end groups. In Table 1 it is shown that the lifetime decreases dramatically after the application of shear. It is

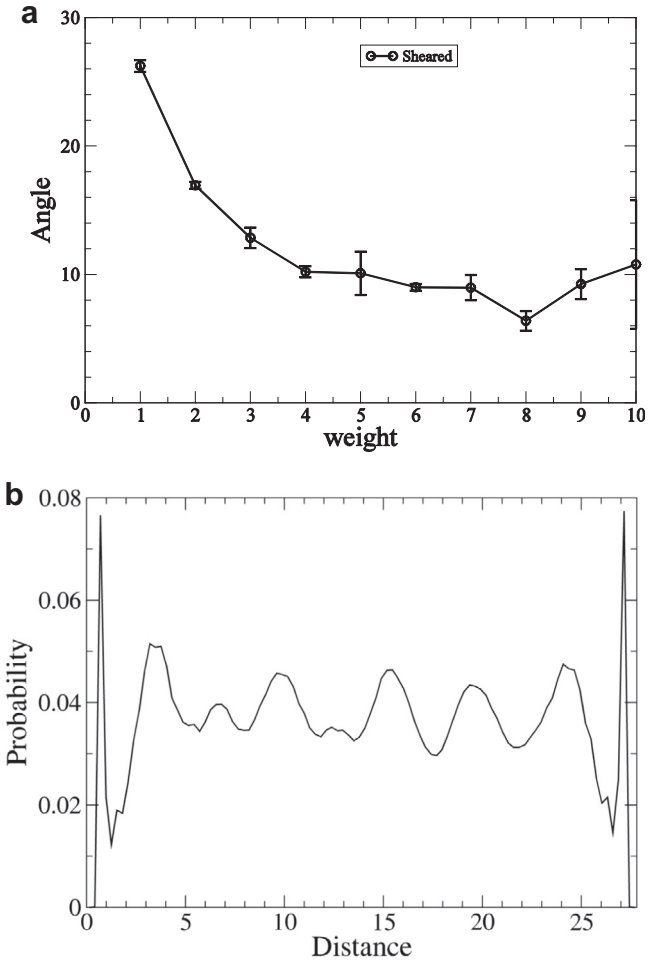

Fig. 8. (a) Orientation versus link weight. The angle is relative to a plane parallel with the walls. (b) Location of end groups as a function of the distance to the bottom (stationary) wall. All data are at $\dot{\gamma} = 3.59 \times 10^{-4}\tau^{-1}$.

slightly shorter in the high shear rate band than in the low shear rate one. The percentage of junctions that survive after a time Δt drops near-exponential with Δt. It is important to note that the junctions that break and reform during this time interval are counted as having survived [20]. The lifetime is defined as the time at which $1/e$ of the number of junctions survive.

All of the above phenomena characterize a difference between the low and high shear rate band. Next, we focus on differences between the sheared and unsheared system. As we will see, the topology of the network differs drastically in a system sheared at a rate for which banding is observed as compared to an unsheared system. It is often mentioned [14,18,17] that under shear a larger fraction of the chains connect with both ends to the same aggregate (loop) instead of bridging between two aggregates (bridge). Our investigation shows that this occurs only for high values of the applied strain. Fig. 6 shows that after application of shear the number of loops only slowly increases. Nevertheless, the topology of the system changes. This can be seen from the decrease of the number of links over time. A link is defined as a connection between two different aggregates. That connection can consist of one or multiple bridging polymer chains. The multiplicity of bridging chains defines the weight of a link. The observed decrease in the number of links over time implies that the average weight of links increases. In other words, under shear the network topology adjusts itself so that larger weight links are formed containing many redundant chains. Fig. 7 shows the link weight distribution.

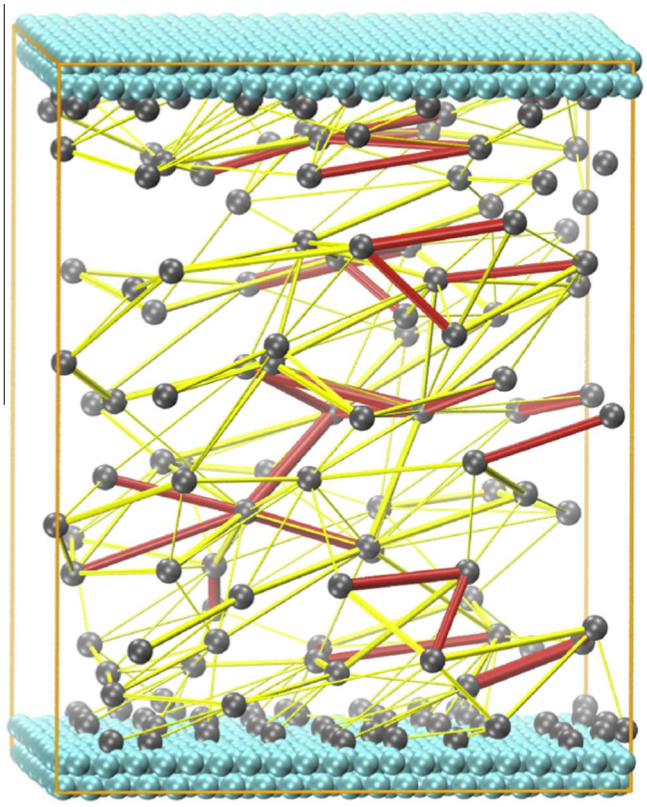

Fig. 9. Snapshot of the data at $\dot{\gamma} = 3.59 \times 10^{-4}\tau^{-1}$. Aggregates are represented by spheres and links by cylinders connecting them. Links of weight 4 and up are red (black) and those of weight three or less yellow (light grey). The radius of a cylinder is also related to the link weight. It can be noticed that the links with a larger weight are orientated preferentially parallel to the wall, in particular in the high shear rate band close to the top wall. (For interpretation of the references to color in this figure legend, the reader is referred to the web version of this article.)

It is observed that the number of chains per link is limited in the unsheared system and links of size 7 or higher are extremely rare. However, as a result of shear, link weight increases dramatically. This appears to be related to the increase in quantity of very large sized aggregates, since there exists a positive correlation between the weight of a link and that of the size of the two aggregates it connects. Note however, only the number of links of weight 3 and up increases under shear. The inset shows the increase in average link weight as a function of strain. Also indicated is the peak that was observed in transient stress response, around a strain of 1.5. The restructuring of the network occurs simultaneously with the stress drop.

Fig. 8a shows the average angle θ between a link of a specific weight and the top wall. The larger the link weight, the more it is aligned with the bounding walls. This alignment does not occur for the unsheared system, for which the orientation of the chains with respect to the walls was random (not shown here). Moreover, a layering of aggregates in planes parallel to the walls is present (Fig. 8b). Hence, we envision a topology in which layers of aggregates are connected by links that contain many chains and are oriented preferentially parallel to the walls. While weaker links with only a few chains, which are more easily broken, connect between these layers. The snapshot of the simulation cell shows this phenomenon (Fig. 9).

4. Conclusions

We applied a wide range of shear rates to the system and observed a region in the shear-stress curve where the stress is relatively independent of shear rate. Within this region, shear banding was observed. The interface between both shear bands fluctuates in position over time. Our results confirm that the lever rule does not strictly hold in telechelic polymer systems. Several microstructural changes were observed between both shear bands. Under shear there is a strong increase in dynamics as indicated by the reduction of the effective lifetime of a junction. This effect is stronger in the high shear rate band and therefore, many aggregates consisting of a single end group are created. This results in more aggregates in the high shear rate band, but since many of them only consist of one end group, the average size is lower. There is a pronounced difference in the topology of the network under shear compared to that of the unsheared network. The aggregate size distribution of the sheared system is very different from that of the unsheared one. The system loses its preference to form aggregates of a specific size as the formation of larger and smaller size aggregates is enhanced. The resulting bimodal distribution is known to be more robust [23] than a single-peaked distribution, suggesting shear induces a structural change into a more resilient network. We also find that aggregates form layers parallel to the bounding walls. Strong links, with high weight, tend to be oriented in these layers. Weaker links, that rupture more easily, are more likely to connect between these layers.

Our results are of importance in light of the recently developed models that describe a stress drop as a result of a decreased bridging factor [14,18,21]. In our studies the number of bridging chains decreases only very gradual over time. Another type of restructuring causes the system to yield. The number of chains that bridge between the same aggregates increases drastically, while the number of links and hence the connectivity of the network drops. Therefore, it is important to take the nature of the links (weight) into account to explain the stress drop. Solely counting the number of bridging chains versus loops is not enough to predict the shear stress.

Current work consists of studying the system under oscillatory shear. This will allow an in-depth study of the dynamic moduli. A time-dependent picture of the topological changes under shear is of interest. In combination with a study of the kinetics of the loops/bridge ratio, oscillatory shear can further reveal the details of these structural changes.

Conflict of interest

There is no conflict of interest.

Acknowledgments

The authors gratefully acknowledge support by a Grant from the NSF under Grant Nos. CHE-0947087 and DMR-1006980. The authors thank Dr. A. Rabinovitch for useful discussions.

References

[1] S. Lerouge, Langmuir 16 (2000) 6464.
[2] M.W. Liberatore, F. Nettesheim, P.A. Vasquez, M.E. Helgeson, N.J. Wagner, E.W. Kaler, L.P. Cook, L. Porcar, Y.T. Hu, J. Rheol. 53 (2009) 441.
[3] M.E. Helgeson, P.A. Vasquez, E.W. Kaler, N.J. Wagner, J. Rheol. 53 (2009) 727.
[4] M.E. Helgeson, M.D. Reichert, Y.T. Hu, N.J. Wagner, Soft Matter 5 (2009).
[5] M.A. Fardin, B. Lasne, O. Cardoso, Phys. Rev. Lett. 103 (2009) 028302.
[6] J.-B. Salmon, A. Colin, S. Manneville, F. Molino, Phys. Rev. Lett. 90 (2003) 228303.
[7] S. Lerouge, M. Argentina, J.P. Decruppe, Phys. Rev. Lett. 96 (2006) 088301.
[8] E. Miller, J.P. Rothstein, J. Non-Newton Fluid 143 (2007) 22.
[9] J.-F. Berret, Y. Séréro, Phys. Rev. Lett. 87 (2001) 048303.
[10] Suzanne M. Fielding, Soft Matter 3 (2007) 1262.
[11] S.M. Fielding, Phys. Rev. Lett. 95 (2005) 134501.
[12] S. Manneville, A. Colin, G. Waton, F. Schosseler, Phys. Rev. E 75 (2007) 061502.
[13] J. Sprakel, E. Spruijt, M.A. Cohen Stuart, N.A.M. Besseling, M.P. Lettinga, J. van der Gucht, Soft Matter 4 (2008) (2008) 1696.

[14] J. Sprakel, E. Spruijt, Martien A. Cohen Stuart, M.A.J. Michels, J. van der Gucht, Phys. Rev. E 79 (2009) 056306.
[15] A.R.C. Baljon, D. Flynn, D. Krawzsenek, J. Chem. Phys. 126 (2007) 044907.
[16] J. Billen, M. Wilson, A. Rabinovitch, A.R.C. Baljon, EPL 87 (2009) 68003.
[17] P.G. Khalatur, A.R. Khokhlov, D.A. Mologin, J. Chem. Phys. 109 (1998) 9602.
[18] K.A. Erk, K.R. Shull, Macromolecules 44 (2011) 932.
[19] K. Kremer, G. Grest, J. Chem. Phys. 92 (1990) 5057.
[20] R.S. Hoy, G. Fredrickson, J. Chem. Phys. 131 (2009) 224902.
[21] K.C. Tam, R.D. Jenkins, M.A. Winnink, D.R. Bassett, Macromolecules 31 (1998) 4149.
[22] M. Wilson, A. Rabinovitch, A.R.C. Baljon, Phys. Rev. E 84 (2011) 061801.
[23] T. Tanizawa, G. Paul, R. Cohen, S. Havlin, H.E. Stanley, Phys. Rev. E 71 (2005) 047101.